IEEE Access
Multidisciplinary | Rapid Review | Open Access Journal

Received August 20, 2020, accepted September 7, 2020, date of publication September 10, 2020,
date of current version September 23, 2020.

Digital Object Identifier 10.1109/ACCESS.2020.3023266

Research on Operation of Low-Speed and High-Torque Module Combined Stator Permanent Magnetic Fault-Tolerant Motor With Unequal Span Winding

BAOPING GAN, BINGYI ZHANG, QIAOSHAN LI, FENG GUIHONG, AND GUANGKUO LI
School of Electrical Engineering, Shenyang University of Technology, Shenyang 110870, China

Corresponding author: Feng Guihong (fenggh@sut.edu.cn)

ABSTRACT Permanent magnetic fault-tolerant motors have been developed rapidly due to their high reliability and have been widely used in many special fields. Compared with the conventional module fault-tolerant motor, the module combined stator permanent magnetic fault-tolerant motor (MCS-PMFTSM) with unequal span winding has two sizes of span coils in each operation module, which realizes the electrical decoupling and mechanical decoupling between the module motors and solves the problem that the span of the double-layer winding of the conventional modular fault-tolerant motor can only be 1. Winding parameters of the unequal span are calculated, on the basis of which the operation performance of MCS-PMFTSM can be analyzed. The performance of MCS-PMFTSM in the normal operation and three failure operations (open circuit failure, Short circuit fault, concurrent failure) are analyzed by finite element method, which proves that it has good fault tolerance. The 12kW100r/min MCS-PMFTSM prototype is tested to verify the correctness of the analysis method and the rationality of the proposed MCS-PMFTSM.

INDEX TERMS MCS,unequal span winding,parameter calculation,fault-tolerant operation.

I. INTRODUCTION

The high-performance permanent magnets generate the main magnetic field of the AC permanent magnet synchronous motor on the rotor. It has high efficiency and power factor, and flexibly designed structure. The speed of the motor changes from hundreds of thousands to dozens of revolutions, and is widely used in direct-drive wind power generation, electric vehicles, servo systems, ship propulsion, direct industrial drive and other fields [1]–[6]. However, the reliability of the motor has put forward higher requirements in many unique applications, such as electric vehicles, ship propulsion, and all-electric aircrafts. Therefore, in recent years, many researchers have turned their interest to study the fault-tolerant motors [7]–[10].

Generally, a typical three-phase permanent magnet motor has no fault-tolerant capacity, because when the one-phase or two-phase winding of the motor has an open or short circuit fault, the stator windings of the motor usually cannot generate the magnetomotive(MMF) force required for the normal operation. Most of the traditional fault-tolerant motors are either multi-phase or redundant motors. The redundant motors can improve reliability through backup fault tolerance [11]–[13]. The disadvantages of the redundant motors are that the system resources are repeatedly configured, they have large size and high cost, and are challenging to apply when the motor volume is demanding, such as electric vehicles and ship propulsion.

Therefore, multi-phase motors, especially 5-phase, 9-phase, and 12-phase motors, are most widely used in recent times [14]–[16]. Multi-phase motor fault-tolerant operation means, when a phase of the motor fails, the stator magnetomotive force equation generated by the remaining normal operational phase windings of the motor meets the stator magnetomotive force equation before its failure. By adding typical constraints, such as minimum copper loss or equal current amplitude to solve the equations, the amplitude and phase of the motor current after the fault are obtained, so that the total magnetomotive force generated by the stator remains unchanged before and after the fault, whereas the normal

The associate editor coordinating the review of this manuscript and approving it for publication was Qinfen Lu.

This work is licensed under a Creative Commons Attribution 4.0 License. For more information, see https://creativecommons.org/licenses/by/4.0/

operation of the motor is maintained [17]. Multi-phase motors can increase the number of phases to ensure the torque output capability of the motor in the event of a fault. However, the control strategy of multi-phase motors is complex, and the cost of the controller is high. In recent years, modular fault-tolerant motors have developed rapidly. Themodular fault-tolerant motor is to modularize the power supply of the whole motor. Each power supply module is an independent motor, and each module motor is controlled according to the control method of the three-phase motor or multiphase motor, and non-interference between the controllers. When a module motor fails, other modules can continue to operate normally with strong fault tolerance [18], [19]. A previous study [20] analysed the fault tolerance performance of permanent magnet - assisted synchronous reluctance motor used in electric vehicles. In the current paper, the whole motor is divided into three independent operational modules by changing the single-layer winding connection and power supply mode to achieve electrical decoupling between the modules. Fault tolerance performance of the motor under open circuit, phase short circuit and inter-turn short circuit faults are also analysed. In a previous study [21], a new type of five-phase modular hub motor is proposed. In the current paper, the fault tolerance of the motor is analysed by the finite element method under four conditions, an open circuit of one phase winding, an open circuit of two adjacent phases winding, an open circuit of two non-adjacent phases winding, and single-phase short circuit. The analysis shows that the motors with different current control strategies can provide satisfactory electromagnetic performance under the above faults and have strong fault tolerance. In a previous work [22], the stator of the traditional U-shaped single-phase permanent magnet synchronous motor with the iron core is added with an auxiliary module to reduce the torque ripple and improve the fault tolerance of the motor. The operating characteristics of the modular servo motors are discussed in another study [23], in which, the servo characteristics and fault tolerance are the optimization targets, and the polar groove coordination is optimized. Furthermore, a new control strategy is proposed to minimize the torque ripple of the motor under one-phase open fault.

The above analysis suggests if the traditional module motor winding is a double-layer structure, the winding span must be unity. Otherwise, the traditional winding structure form makes the winding between modules cross-coupled, which cannot realize the modular operation of the motor, and undoubtedly limits the application range of the modular fault-tolerant motor. At present, the low-speed high-torque direct-drive motor, especially the high-power motor in the electric ships' propulsion systems still adopts the multi-phase fault-tolerant motor. There are two main reasons for using a multi-phase motor. One is that the low-speed and high-torque direct-drive motor has immense power to reduce the current of the controller. Furthermore, it is used to improve the fault tolerance of the motor when the span of the traditional winding structure is not unity. In such a case, it is impossible to realize the modular power supply operation of the motor. Moreover, there are few reports on the application of low-speed high-torque permanent magnet module motors.

Based on the above backdrop, a module combined stator permanent magnetic fault-tolerant motor (MCS-PMFTSM) with unequal span winding is proposed [25]. There are large and small span windings in the stator windings to realize the electrical and mechanical decouplings of the module motors. Each module is using an independent inverter power supply to give motor a strong fault tolerance. The MCS-PMFTSM not only solves the problem that the span of the double-layer winding of the conventional modular fault-tolerant motor can only be unity, but also solves the problems of processing, transportation, installation and maintenance caused by the large volume of the high-power direct-drive motor. The high-power direct-drive motor adopts the combined stator structure of unequal span module. The voltage and current of each module motor are small. The capacity of the controller will not be increased, and the control mode of each module adopts the traditional three-phase motor control method. Furthermore, the control strategy is simpler than the traditional multiphase motor.

Traditional modular fault-tolerant motors can only use fractional slot concentrated windings or single-layer windings for electromagnetic decoupling winding structure between modules. For some high-speed fault-tolerant motor applications such as electric vehicles, if the fractional slot concentrated winding is used, the motor has a large number of poles and high frequency, especially when the motor runs in the constant power range, the motor frequency will be higher, the iron loss will increase, and the efficiency will be reduced. This way sacrifices the efficiency to improve the fault tolerance of the motor, which is not advisable. Andthe single-layer winding back EMF has poor sinusoidal properties and large torque ripple, which is not suitable for large direct-drive motors. Compared with traditional modular motors, MCS-PMFTSM uses new unequal-span windings to achieve decoupling operation between modules. In motor design, winding of the motor is no longer limited to specific structures, and more choice of pole slot coordination can be made. So MCS-PMFTSM has better performance, and can be used in more applications.

Based on a previous study [25], this article further investigates the operation of MCS-PMFTSM. The winding structure and fault tolerance principle of MCS-PMFTSM are introduced in Section I. Since there are two kinds of span coils in the motor winding, the parameters of the unequal span winding are calculated, and the influence of the unequal span winding on the normal operation of the motor is analysed in Section II. The operational performance of the motor under various faults are analysed by finite element method and optimized based on genetic algorithm using the three common faults (open phase winding, short circuit of phase winding and concurrent faults) in the motor and described in Section III. Consequently, a prototype was made, and an experimental platform was built, which is described in Section IV of this

manuscript. Both the theoretical analysis and experiments proved the rationality of the MCS-PMFTSM.

II. MCS-PMFTSM WINDING STRUCTURE AND FAULT TOLERANCE PRINCIPLE

A. MCS-PMFTSM WINDING STRUCTURE

Since each module operates independently of the power supply, the stator of each independently operated module motor must meet the basic principles of rotating electrical machine operation. According to the motor theory, the smallest independent motor is a unit motor, due to which, each module motor must be composed of an integer number of unit motors. Considering the general situation, each running module can be composed of different unit motors.

Suppose the number of slots in a motor stator is Q and the number of slots in a unit motor is Q_0. There are n operating modules in total. The i-th module consists of k_i unit motors. ($k_i \in Z+$).

$$Q_i = k_i Q_0 \tag{1}$$

The MCS structure does not change the number of slots and poles of the original motor, so the total number of slots of the motor does not change after separation.

$$\sum_{i=1}^{n} k_i Q_0 = Q \tag{2}$$

According to the unit motor theory, the Equation (2) can be written as

$$\sum_{i=1}^{n} k_i = \frac{Q}{Q_0} = t \tag{3}$$

t is the number of unit motors.

Eq. (3) shows that the number of independent operation modules that can be split by the entire motor is related to the number of unit motors of the original motor.

In order to provide electrical decoupling between the modules, windings across different modules should be inversely embedded in the module. In order not to affect the electromechanical energy conversion, the effective part of each module winding must constitute a three-phase symmetrical winding. According to the winding theory, the pitch of the large-span coil is as follows.

$$y_2 = k_i Q_0 - y_1 \tag{4}$$

y1 is the pitch of the small-span coil.

$$y_1 = \frac{5}{6}\frac{Q}{2p} \tag{5}$$

p is the number of pole pairs of the motor.

In order to make MCS-PMFTSM operate symmetrically on the circumference, the MCS is designed to ensure that each module k_i is the same. In particular, when k_i is equal to 1, for maximum splitting, each running module is a unit motor.

30-pole 72-slot winding connection diagram as shown in Figure 1.

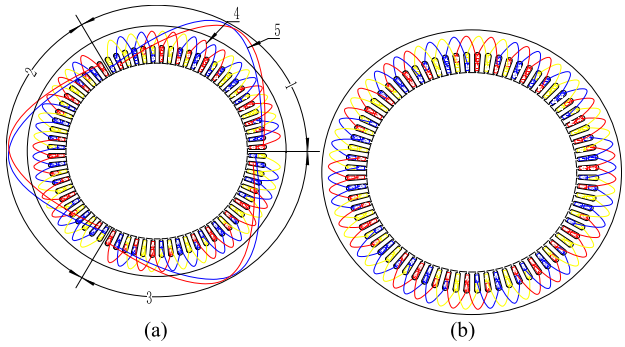

FIGURE 1. Windings of PMSM. (1-module1; 2-module2; 3-module3; 4-small span winding 5-large-span winding); (a) Windings of PMFTSM; (b) Winding of traditional PMSM.

TABLE 1. Parameters of the invesgated machine.

Parameter	Value
Rated power/kW	12
Rated speed/r/min	100
Slot/pole	72S/30P
No-load back EMF/V	208.5
Number of modules	3
Small span	2
Large span	22

The currents are fed into the windings A1, A2 and A3, and the radial air gap flux density waveform generated by the stator MMF is calculated using the finite element method (FEM). The results are shown in Fig. 2.

The radial air gap flux density waveform generated by the stator MMF of the MCS-PMFTSM is exactly the same as the radial air gap flux density waveform generated by the traditional 30-pole 72-slot motor.

It can be seen from the above analysis that, compared with the traditional coil, the large-span coil has only changed in the end connection mode, and the current phase and direction of the conductor in the stator slot have not changed. The effective part of the motor for electromechanical energy conversion is the length of the core. The ends are only connected, while each operating module is symmetrically distributed on the circumference, so the unequal span winding will not affect the electromechanical energy conversion of the entire motor system.

According to the above MCS-PMFTSM design principle, a 12kw100r/min prototype is manufactured.Primary parmeters of MCS-PMFTSM are as follows.

B. MCS-PMFTSM FAULT TOLERANCE PRINCIPLE

MCS-PMFTSM unequal span realizes the mechanical and electrical decouplings of the motor stator module. An independent controller is used to drive the module motor between the modules, whereas each controller does not interfere with the other. The MCS-PMFTSM control system is shown in Fig. 3.

When a certain motor stator module or driver fails, the fault part will be removed as a whole without affecting the other

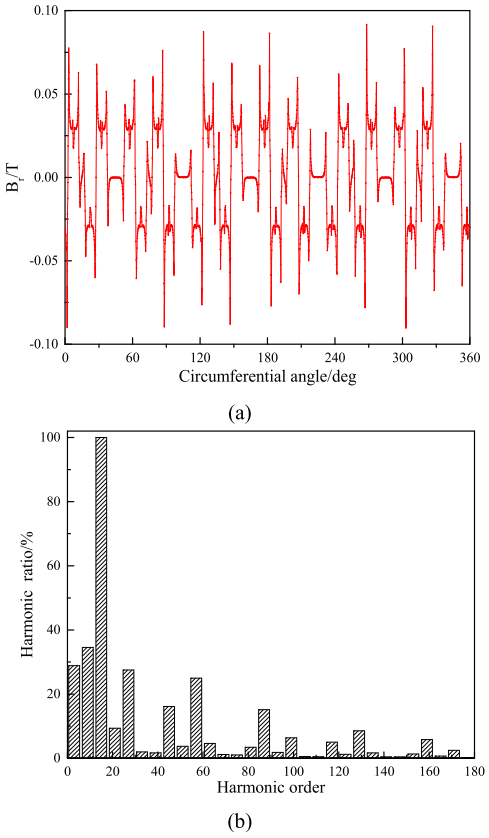

FIGURE 2. MCS-PMFTSM A-phase radial air gap flux density: (a) Radial air gap flux density; (b)FFT.

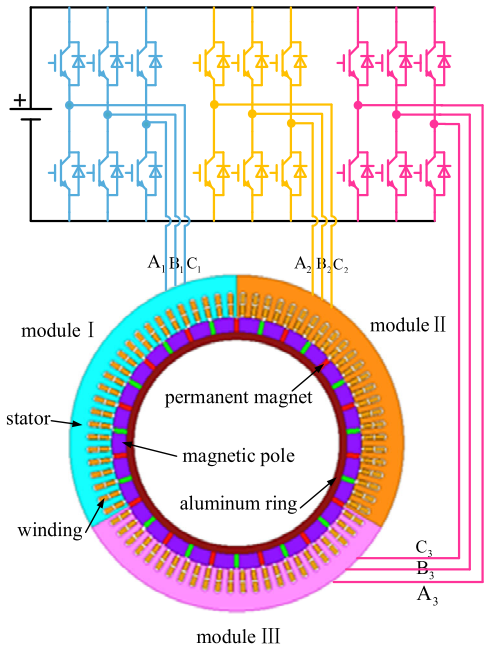

FIGURE 3. MCS-PMFTSM power supply system.

normally operating modules, which gifts it high fault tolerance. The current and power of each module driver are reduced compared to the traditional driving mode.

According to the MCS-PMFTSM fault tolerance principle, when a certain module fails, the faulty module will be removed as a whole. However, if the load torque of the motor remains unchanged at this time, the overall output power of the motor will decrease, and the remaining normal modules will work in an overload state. Additionally, the motor current will become larger. However, when the motor has a short-circuit fault, there is always a short-circuit current in the short-circuit module. When the motor fails, the winding current is too large. In such a case, the motor loss increases, and the temperature rises. If the temperature is too high, the other normally operating modules will malfunction or even demagnetize the magnet, which will affect the stable operation of the motor. Therefore, it is necessary to calculate the maximum operating current and the operating time when the motor fails. Unlike the open circuit fault, when there is a short circuit fault, there is always copper loss in the module, and the short circuit current will produce a braking torque that further weakens the output torque of the motor. Therefore, when calculating the maximum running current and the longest-running time under the fault state of the motor, there is short-circuit current in the fault module (the short-circuit fault in this article is defined as the phase winding short-circuit situation).

Based on the electromagnetic field-temperature field bidirectional coupling method [26], under the condition that the maximum operating temperature of the motor is not exceeded, it is determined that, when the motor fails to run for 40 min, the maximum phase current allowed in the winding of the module motor is 1.5 times of the rated current. When the motor fails to run for 20 min, the maximum phase current allowed in the motor winding of the module is 2.8 times of the rated current. The fault-tolerant motor designed in the current paper requires the minimum time of fault operation to be 20 min.

III. PARAMETER CALCULATION OF UNEQUAL SPAN WINDING

Compared with the traditional motor winding, unequal span winding has two kinds of span windings. This section calculates the resistance and inductance of the unequal span windings to analyze the effect of unequal span winding structure on normal operation of a single independent module motor and provides winding parameters for the operational analysis of the entire MCS-PMFTSM.

A. RESISTANCE CALCULATION

Due to the low running frequency of the motor and the winding using the multiple conductors in parallel, the AC resistance was ignored, and only the DC resistance was considered. The DC resistance of phase winding can be calculated by Eq. (6) [27] .

$$R = \rho_0(1+\alpha t)\frac{lN_s}{\pi a \sum_{i=1}^{n} N_{ti}(\frac{d_i}{2})^2} \tag{6}$$

where ρ_0 is the resistivity of the conductor at 0 °C, t is the temperature of the conductor, α is the temperature coefficient of the resistivity of the conductor, N_s is the number of series turns of each phase winding, a is the number of parallel branches of the winding. N_{ti} is the number of parallel windings of the i-th wire gauge, d_i is the i-th wire gauge conductive diameter, and l is the length of the winding.

After calculations, it was found that the three-phase resistance of the MCS-PMFTSM at 30 °C is as follows:

$$R_A = R_C = 0.91\Omega \quad R_B = 0.75\Omega$$

The resistance of Phases A and C is higher than that of Phase B due to the existence of large-span coils in Phases A and C, whereas the coil length is large, due to which, the resistance is significantly large.

B. INDUCTANCE CALCULATION

Since the span of the same phase winding in the module motor may not be equal, the inductance parameters of a single-coil are calculated when calculating the inductance parameters. The inductance of the coil on a branch circuit is calculated according to the connection relation of the coil on the same circuit.

Self-inductance can be approximated using the analytical methods. In the unequal-span winding, the overlap of the stator ends of the motor is complicated due to the existence of a large-span, which is difficult to obtain using the analytical method. Therefore, the mutual inductance is obtained using the FEM.

C. SELF-INDUCTANCE CALCULATION

Moreover, self-inductance is divided into main inductance and leakage inductance. In the stator coil of the motor, the leakage inductance mainly includes slot leakage inductance and winding end leakage inductance. According to the analytical method provided in a previous work [27], the coil inductance is calculated.

1) CALCULATION OF MAIN INDUCTANCE

The flux line generated by the main inductance passes through the air gap from the stator to rotor and then, returns from the rotor to the stator. The calculation equation is given by Eq. (7).

$$L_m = \frac{4\mu_0 k \tau_t l_{ef}}{\pi(\frac{h_m}{\mu_r} + k_c\delta)}(k_{ws_1}N)^2 \tag{7}$$

where μ_0 is the permeability in vacuum, N is the number of coil turns, and k_{ws1} is the fundamental winding factor. Furthermore, L_{ef} is the motor core length, τ_t is the stator tooth pitch, k is the number of teeth contained in the coil, h_m is the thickness of the permanent magnet in the magnetization direction, μ_r is the relative permeability, and δ is the air gap length. Additionally, k_c is the Carter coefficient, and the correlation used is given by Eq. (8).

$$k_c = \frac{\tau_t}{\tau_t - \frac{4\delta}{\pi}\left[\frac{b_0}{2\delta}\arctan\frac{b_0}{2\delta} - \ln\sqrt{1+(\frac{b_0}{2\delta})^2}\right]} \tag{8}$$

where, b_0 is the stator notch width.

2) CALCULATION OF STATOR SLOT LEAKAGE INDUCTANCE

The slot leakage inductance is generated by the current conductor in the stator slot, and its value is related to the stator slot shape and the phase of the conductor in the slot. In this article, the slot shape of the motor stator is a pear-shaped slot, whereas the slot dimensions are presented in Table 2. For the two types of span coils, only the end connection is different, and the current amplitude and the phase in the effective part of the conductor in the slot are precisely the same as the traditional permanent magnet motor. Therefore, the slot leakage permeability of the two-span coils is the same. The double-layer short-distance winding slot leakage permeance factor can be calculated using Eq. (9)

$$\lambda_{\delta s} = \frac{3\beta}{4}(\frac{h_0}{b_0} + \frac{2h_1}{b_0+b_1}) + \frac{\beta(9\beta+7)(K_{r1}+K_{r2})}{16\left[\frac{\pi}{8\beta} + \frac{(1+\alpha)}{2}\right]^2}. \tag{9}$$

TABLE 2. Stator slot parameters.

Parameter	Value/mm	Parameter	Value/mm
b01	4	h0	1
b1	8.3	h1	1.24
b2	11.02	h2	31.26

β is the short distance coefficient, which is 5/6 in this article. Where (10), as shown at the bottom of the page.

According to the definition of inductance, the leakage inductance of the motor slot is given by Eq. (11).

$$L_{\delta s} = \mu_0 N^2 l_{ef} \lambda_{\delta s} \tag{11}$$

$$\begin{cases} K_{r1} = \frac{1}{3} - \frac{1-\alpha}{4}\left[\frac{1}{4} + \frac{1}{3(1-\alpha)} + \frac{1}{2(1-\alpha)^2} + \frac{1}{(1-\alpha)^3} + \frac{\ln\alpha}{(1-\alpha)^4}\right] \\ K_{r2} = \frac{2\pi^3 - 9\pi}{1536\gamma^3} + \frac{\pi}{16\gamma} - \frac{\pi}{8(1-\alpha)\gamma} - \left[\frac{\pi^2 + 8\pi\gamma}{64(1-\alpha)\gamma^2}\right]\ln\alpha \\ \alpha = \frac{b_1}{b_2} \\ \gamma = \frac{h_2}{b_2} \end{cases} \tag{10}$$

3) LEAKAGE INDUCTANCE OF END-WINDING CALCULATION

The end-winding leakage inductance is caused by the magnetic flux leakage at the end of the stator winding of the motor, whereas the end-winding leakage permeance factor can be calculated using Eq. (12).

$$\lambda_{\delta e} = \frac{0.67 l_{ed} - 0.43 k \tau_t}{l_{ef}} \tag{12}$$

where l_{ed} is length of winding end.

According to the definition of inductance, in a coil, end-winding leakage inductance can be expressed using Eq. (13).

$$L_{\delta e} = \mu_0 N^2 l_{ef} \lambda_{\delta e} \tag{13}$$

The coil inductance is the sum of the above three inductances.

The self-inductance of the small-span coil is as follows.

$$L_s = L_m + 2L_{\delta s} + L_{\delta e} = 4.95\text{mH}$$

The self-inductance of the large-span coil is as follows.

$$L_l = L_{ml} + 2L_{\delta s} + L_{\delta e} = 23.62\text{mH}$$

D. MUTUAL INDUCTANCE CALCULATION

According to the definition of incremental inductance, when the rotor is in a certain position, the mutual inductance of the coils is given by Eq. (14).

$$M_{12} = \frac{\psi_2 - \psi_0}{I} \tag{14}$$

In order to verify the accuracy of self-inductance calculated using the above analytical method, the FEM is used to calculate the coil self-inductance. The calculation equation is given by Eq. (15).

$$L_{11} = \frac{\psi_1 - \psi_0}{I} \tag{15}$$

where ψ_0 is the flux linkage of No. 1 coil turn chain under the action of permanent magnets, ψ_1 is the flux linkage of the turn chain of the No. 1 coil with the input current in the No. 1 coil, and ψ_2 is the flux linkage of the turn chain of No. 2 coil with the input current in the No. 1 coil.

By calculating the flux linkage of the motor rotor at different positions through the 3D FEM and substituting it into Eqs. (14) and (15), the mutual inductance and self-inductance are calculated. The finite element model is shown in Fig. 4.

The finite element calculation results are shown in Figure 5.

According to the FEM calculations, the self-inductance of the large-span coil is 23.85 mH, whereas the self-inductance of the small-span coil is 5.05 mH, which is similar to the analytical calculations.

As can be seen from Fig. 5, the self-inductance and mutual inductance of the coil are not constant, and there are periodic fluctuations. There are two main reasons. One is that the tangential embedded rotor structure of the motor leads to the asymmetry of the magnetic circuit of the d-axis and the q-axis. The other is that the main magnetic field of the motor is caused by the saturation effect.

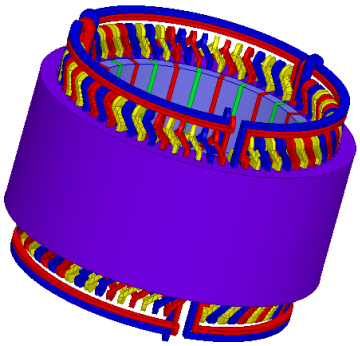

FIGURE 4. MCS-PMFTSM 3D model.

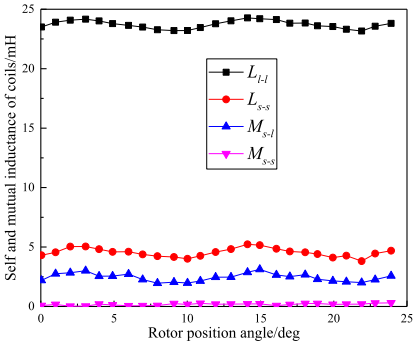

FIGURE 5. Coil self-inductance and mutual inductance curves L_{s-s}- self-inductance between the small-span coils L_{l-l}- self-inductance between the large-span coils M_{s-s}- mutual inductance between the small-span coils M_{l-s}- mutual inductance between the large-span coils and small-span coils.

Using the above method, the self-inductance and mutual inductance of all coils in a module can be calculated independently. According to the connection relationship between the coils, the three-phase inductance parameters of the motor in a module are calculated, and the results are shown in Table 3.

TABLE 3. Three-phase winding inductance parameters/mH.

	A- Phase	B- Phase	C- Phase
A- Phase	41.82	-5.95	-9.92
B- Phase	-5.95	34.75	-5.42
C- Phase	-9.92	-5.42	41.83

According to the calculation results, the self-inductance of the Phase B winding and the mutual inductance between the Phase B winding and the Phases A and C winding are both small, because there is no large-span coil in the Phase B winding.

According to the phase resistance and phase inductance calculated above, the three-phase impedance of each module of MCS-PMFTSM is as follows.

$$\begin{cases} Z_A = R_A + j2\pi f L_A = 4.082\angle 56.69^\circ \\ Z_B = R_B + j2\pi f L_B = 4.475\angle 57.73^\circ \\ Z_C = R_C + j2\pi f L_C = 4.804\angle 56.70^\circ \end{cases} \tag{16}$$

where f is the rated frequency of the motor.

Due to the existence of large-span coil, the impedance value and the phase of coil are different from other two-phase windings. When the motor is running, the three-phase current in each module is slightly different, and the phase will be offset. Nevertheless, for the whole motor system, this asymmetric winding is evenly distributed along the circumference, and will not cause excessive local losses.

IV. MCS-PMFTSM OPERATION ANALYSIS

In this section, the operation of MCS-PMSM is analyzed using the FEM. The normal operation and fault operation of the motor, includes three common faults in the motor, namely the open circuit, the phase winding short circuit, and the concurrency fault.

A. MCS-PMFTSM NORMAL OPERATION ANALYSIS

The above analysis shows that there are two kinds of span coils in MCS, and the internal three-phase winding parameters of each operating module are asymmetric. Therefore, the influence of unequal span winding on the motor operation is analyzed during the normal operation of the motor.

When the motor runs without load, the no-load loss of the motor is ignored, and the power angle of the motor is 0. And when the motor output rated torque, the power angle of the motor becomes 30.5°. Suppose that the power supply of each module is the same three-phase ideal symmetrical voltage source, then the current of each phase of a module is shown in Fig. 6.

When the motor is running without load, the phase current in a module is given by the correlations: $I_A = I_C = 0.68A$, $I_B = 0.73A$. For the output rated torque of the motor, the phase current in a module is given by the correlations: $I_A = I_C = 7.17A$, $I_B = 7.31A$.

From the above analysis, it can be seen that there are two coils with large and small spans in a single module motor, which results in unequal three-phase winding parameters. When the motor is running, the amplitude of the three-phase current in the module is not equal, and the phase is also offset. Although the three-phase current in a module is unbalanced, the difference in the effective values of the current between the three phases is very small, which will not cause local overheating of the motor. For the whole motor system, each module is identical and symmetrically distributed along the circumference. Therefore, the unequal span coils are asymmetric for the internal operation of a single module motor. However, for the whole motor system, the operation is symmetric.

The asymmetric operation of a modular motor is mainly because the number of large-span coils cannot be evenly distributed to the three phases. Therefore, the three-phase winding parameters are asymmetric. According to the design principle of unequal span windings, the number of large-span coils in a module is the span of small-span coils. Therefore, in order to eliminate the asymmetric operation inside a single module motor, caused by large-span coils, following methods can be adopted. One is that, during designing, the span of the small-span coil can be designed as a multiple of 3. The other is that, the inductance is connected in series with the phase winding without or with a small number of large-span coils to balance the three-phase winding parameters.

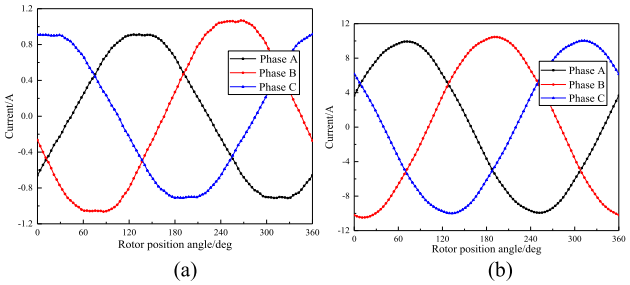

FIGURE 6. Current of a module motor: (a) No-load curren; (b) Rated current.

The inductances are connected to the B-phase winding of each module to balance the three phases. For the output rated torque of the motor, the torque ripple is only 0.93%. This is because the motor uses fractional slot winding to make the entire motor system run smoothly. The output torque of the whole motor system is shown in Fig. 7.

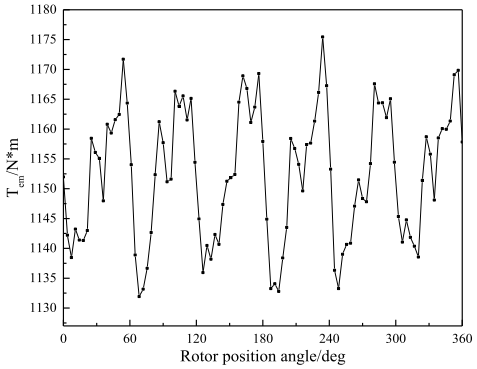

FIGURE 7. Rated torque of motor under normal operation.

B. MCS-PMFTSM OPEN CIRCUIT FAULT OPERATION ANALYSIS

Here, the series inductance and the three-phase impedance balance are included in the fault-tolerance analysis.

1) ONE MODULE OPEN CIRCUIT FAILURE

An open-circuit fault occurs in a module of the motor, and the faulty module is completely removed. The current in this module immediately reduces to 0. The current in the other two modules remains unchanged, and the output torque of the motor is shown in Figure 8. The average torque is 762.7 N*m, which is slightly lower than 2/3 of the rated torque. Among them, the 2nd, 4th, 6th, and 12th harmonic torque contents increased, and the torque ripple became larger, which is caused by the unbalanced radial force after the open circuit fault. The output torque of the harmonic motor analysis, is shown in Figure 12.

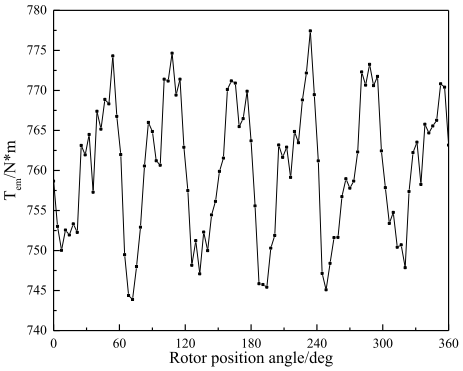

FIGURE 8. Output torque of the motor under open fault of one module (Phase current unchanged).

In order to make the motor output rated torque in case of an open circuit failure of a module, the stator current amplitude of the other two modules is increased by 1.5 times. The output torque is shown in Fig. 9.

As shown in Fig. 9, the output torque of the motor is 1145.2 N*m, reaching the rated torque. With the increase in the phase currents of the remaining two modules, the unbalanced radial force wave caused by the open circuit fault becomes larger, whereas the torque ripple of the motor increases to 7.55%. The torque loss of the fault module can be compensated by increasing the current amplitude of the other two modules.

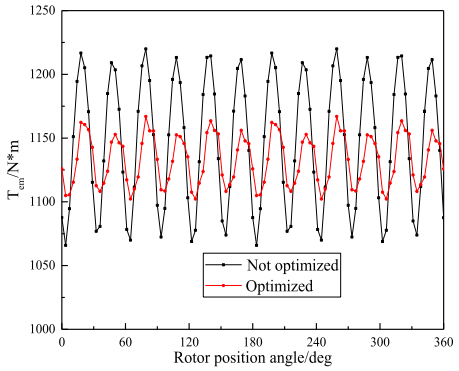

FIGURE 9. Rated torque output of the motor under open circuit fault of one module.

The torque expression of the permanent magnet motor is given by Eq. (17) [28].

$$T_e = p[i_s\psi_f \sin\beta + \frac{1}{2}(L_d - L_q)i_s^2 \sin 2\beta] \qquad (17)$$

where is is the stator current in d-q coordinate system; p is pole pairs; ψ_f is the permanent magnet flux linkage; β is the angle between current vector and q- axis in d-q coordinate system; L_d and L_q are the d-axis and q-axis inductance of the stator winding.

In addition to being related to the amplitude of the phase current, the output torque of the motor also depends on the angle between the stator current vector and the q-axis. The motor stator current amplitude remains unchanged. However, within a certain range, the stator current angle can increase the reluctance torque of the motor. Therefore, the total output torque of the motor increases. When one module open circuit fails, the stator current amplitude is analyzed using the FEM within the range of 1.3 - 1.9 times of the rated current. Due to this reason, the motor output rated torque, the torque ripple, and the phase current angle change, as shown in Figure 10.

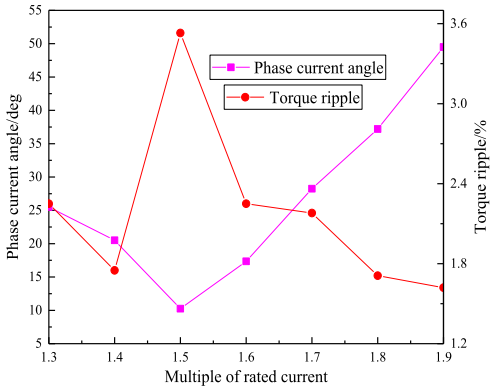

FIGURE 10. The relationship between stator phase current amplitude, phase current angle and torque ripple under rated torque output of the motor.

For the output rated torque of the motor, as the current amplitude increases, the torque ripple first decreases, then increases and finally, decreases again. At 1.3 - 1.5 times of the rated current torque, the ripple reduces, followed by an increase. This is because when the current is small, the reluctance torque accounts for a high proportion, which causes the torque ripple to increase.

As the current amplitude increases, the proportion of the reluctance torque decreases, and the torque ripple also decreases. As the current amplitude increases above 1.5 times of the rated current, the phase current angle becomes larger, and the torque ripple becomes larger, followed by a decrease. This is because, the amplitude of phase current increases, while the unbalanced radial force wave increases. Meanwhile, the torque ripple increases. As the phase current angle continues to increase, the d-axis demagnetization magnetomotive force increases. The unbalanced radial force wave decreases, and the torque ripple decreases. When the amplitude of the phase current is less than 1.5 times of the rated current, the stator phase current angle increases, and the reluctance torque increases. However, the minimum value of the torque ripple is less than 1.5 - 1.7 times of the rated current. The increase in the reluctance torque will cause the motor torque ripple to become larger. When the reluctance torque causes the torque ripple value to be less than the torque ripple caused by the unbalanced radial force, the total torque ripple of the motor decreases. When the current increases, the motor loss becomes larger, which is not conducive to the operation of the motor. Considering the torque ripple and

motor loss comprehensively, there must be a minimum torque ripple between 1.3 - 1.5 times of the rated current.

Genetic algorithm is a kind of reference to the biological evolution law of the biological world, and is a kind of global optimization search method. Genetic algorithm realizes the characteristics of biological evolution, group competition, natural selection, heredity, mutation, etc. through computer simulation, and is especially suitable for optimization of combination variables. So genetic algorithm is used to optimize the phase current in this article.The appropriate optimization target is selected according to different fault conditions. Generally speaking, the optimized objective function is the minimum torque ripple. However for extreme concurrent faults such as the open circuit of one module and the three-phase short circuit of another module mentioned later in this article, the objective function is the maximum value of output torque in order to make the output torque as large as possible. According to the electromagnetic torque expression of the permanent magnet motor, the phase current amplitude and the phase current angle are selected as the optimized variables. In order to reduce the search range of the genetic algorithm, the finite element method is used to estimate the range of phase current amplitude corresponding to rated output torque or maximum output torque in different fault conditions.

Based on the above ideas, the mathematical model of genetic algorithm is established, the established mathematical model is combined with finite element method, and the final results are calculated by finite element method.

For a module open circuit, the objective function is the minimum torque ripple, and the mathematical model is given by Eq. (18).

$$\begin{cases} \min f(x) = \dfrac{T_{\max} - T_{\min}}{2T_{avg}} \times 100\% \\ x = (I, \beta) \\ s.t. 1.3I_N \le I \le 1.5I_N; 0° \le \beta \le 90°; \\ 1000 \le T_{avg} \le 1147 \end{cases} \tag{18}$$

The optimization results show that the stator current amplitude is 1.42 times of the rated current, and the phase current angle is 20.5°. The torque ripple is at least 3.85%. The output torque is shown in Fig. 9.

2) TWO MODULES OPEN CIRCUIT FAILURE

Two modules of the motor have open circuit faults, while the current in the remaining one module remains unchanged. The output torque of the motor is shown in Figure 11. The average torque is 380.3 N*m, which is slightly less than the 1/3 of the rated torque.

If the stator current amplitude of the other module is changed to 3.3 times, the rated torque of the motor can be the output, as shown in Figure 13. Meanwhile, the torque ripple is 18.8%, and the copper consumption is 3.63 times of the original, which is not conducive to the motor failure operation. The optimization method mentioned above is used for optimization, and the mathematical model is given by

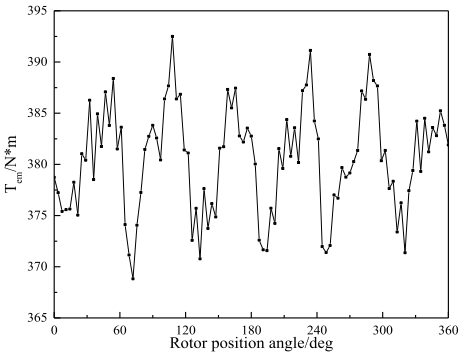

FIGURE 11. Output torque of the motor under open fault of two modules (Phase current unchanged).

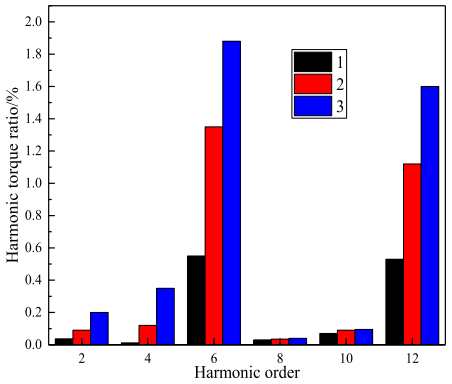

FIGURE 12. Torque harmonic: 1- Normal operation; 2-Open-circuit fault in one module; 3- Open-circuit fault in two modules.

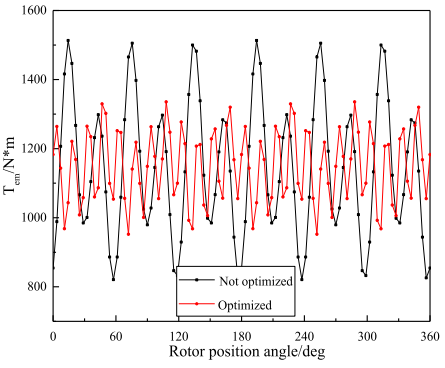

FIGURE 13. Rated torque output of the motor under open circuit fault of two modules.

Eq. (19).

$$\begin{cases} \min f(x) = \frac{T_{\max} - T_{\min}}{2T_{avg}} \times 100\% \\ x = (I, \beta) \\ s.t. 1.9I_N \le I \le 2.8I_N; 0° \le \beta \le 90°; \\ 1000 \le T_{avg} \le 1147 \end{cases} \tag{19}$$

When the stator current amplitude is 2.5 times the rated current and the phase current angle is 46.6°, the motor can produce the rated torque, as shown in Figure 12. The torque ripple was reduced to 9.26%.

The analysis of the above results shows that MCS-PMFTSM can operate in fault tolerance when one or two modules are open-circuited.

3) MCS-PMFTSM SHORT CIRCUIT FAULT OPERATION ANALYSIS

It has been reported that the short-circuit of the phase winding itself is more harmful than the short-circuit between the phases. Therefore, the short-circuit faults in the current paper are based on the short-circuit of the phase winding itself.

Different from the open circuit fault, when the motor phase winding short-circuit fault occurs, the short circuit current still exists in the fault module after the fault module is cut out as a whole. Short-circuit current of a module three-phase winding is shown in Fig. 14.

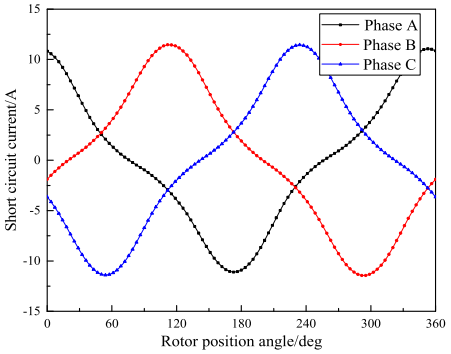

FIGURE 14. Three-phase short-circuit current of a module motor.

The effective value of short-circuit current is 6.52A, which is slightly less than the rated current. In case of short-circuit fault of the motor, the motor will not be damaged due to overheating caused by the short-circuit current. Under short circuit condition, the phase current in the normal winding remains unchanged, the output torque of the motor is shown in Fig. 15.

The average torque value is 613.9 N*m, which is less than 2/3 of the rated torque. This is because the generated braking torque due to short-circuit winding current during one-phase short circuit makes the average output torque of the motor less than that of the one-phase open circuit. The torque ripple is 14.58%, which is higher than the one-phase open circuit. This is because the unbalanced radial force generated by the short-circuit current increases the amplitude of the 2, 4, and 6 harmonics in the electromagnetic torque and causes the torque ripple to increase.

When different numbers of phase windings of the module motor are short-circuited, the short-circuit current has different effects on the output torque of the motor. In this article, when different numbers of phase windings are short-circuited, the output torque and harmonic torque ratio of the motor are studied (the positional order of the short-circuited phase windings is A_1, A_1B_1, $A_1B_1C_1$, $A_1B_1C_1A_2$, $A_1B_1C_1A_2B_2$, $A_1B_1C_1A_2B_2C_2$). The results are shown in Fig. 16.

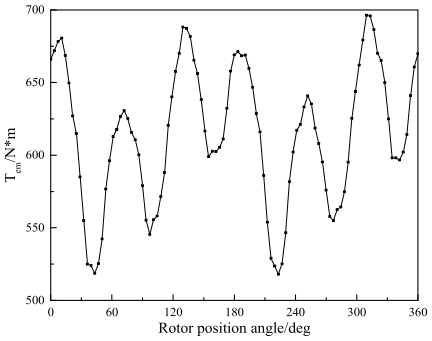

FIGURE 15. Output torque of the motor under three-phase short circuit of one module (Phase current unchanged).

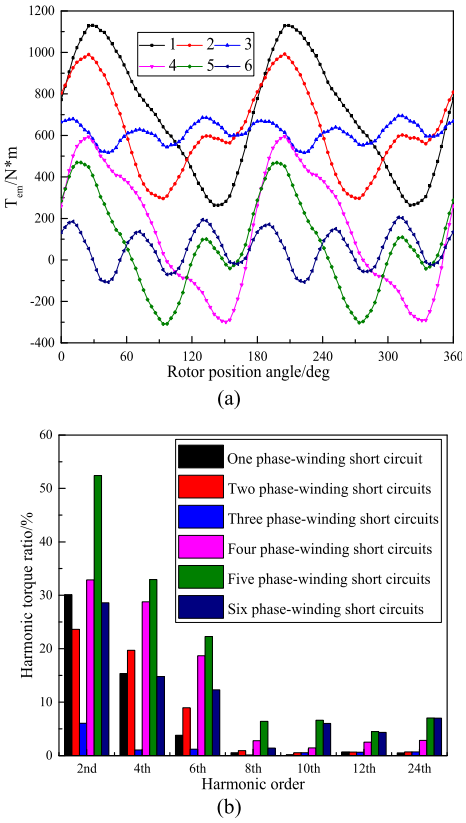

FIGURE 16. Output torque of the motor with different number of short-circuit windings(Phase current unchanged): (a)Torque;waveform; (b)FFT. 1- One phase-winding short circuit Tavg = 699.4N*m; 2-Two phase-winding short circuits Tavg = 628.6N*m; 3-Three phase-winding short circuitsTavg = 612.8 N*m; 4- Four phase-winding short circuits Tavg = 146.5 N*m; 5- Five phase-winding short circuits Tavg = 73.5 N*m; 6- Six phase-winding short circuits Tavg = 54.7 N*m.

When the short-circuit fault occurs in a certain number of phase windings of the motor, the output torque of the motor becomes negative at some moments, which is caused by the braking torque generated by the short circuit.

According to the above analysis, it can be seen that, when the symmetrical short circuit (three-phase winding or six-phase winding short circuits) occurs in the module motor, the proportion of each harmonic in the output torque of the motor is less than that of the asymmetric short circuit.

Additionally, the output torque harmonic content in the condition of six phase-winding symmetrical short circuits is higher than that in the condition of three phase-winding symmetrical short circuits.

This is because, the motor phase winding is asymmetrically short-circuited, while the magnetic field generated by the short-circuit current in the winding interacts with the rotor magnetic field to produce a pulsating braking torque. The motor phase winding occurs symmetrically short- circuited, whereas the short-circuit current in the winding interacts with the rotor magnetic field to produce a constant braking torque. The output torque of the motor is the superposition of the driving torque and the braking torque. Meanwhile, the symmetry of the unbalanced radial force generated by the motor in the symmetric short-circuit is better than that generated by the asymmetric short-circuit. Therefore, when the motor operates in the asymmetrical short-circuit state, the output torque harmonics accounts for a large proportion. As the number of symmetrical short-circuit windings increases, the effect of the unbalanced radial force generated by the motor on the output torque of the motor becomes greater. Therefore, the output torque harmonic content for the six phase-winding symmetrical short-circuits is higher than that for the three phase-winding symmetrical short-circuits.

With a module three-phase short-circuit fault as the research object, the optimization mathematical model is given by Eq. (20).

$$\begin{cases} \min f(x) = \dfrac{T_{\max} - T_{\min}}{2T_{avg}} \times 100\% \\ x = (I, \beta) \\ s.t. 1.6I_N \le I \le 1.9I_N; 0° \le \beta \le 90°; \\ 1000 \le T_{avg} \le 1147 \end{cases} \tag{20}$$

After optimization, the current amplitude is 1.65 times of the rated current, whereas the phase current angle is 17.3° (Fig. 17). The minimum torque ripple is 11.53%, and the average output torque is 1052.5 N*m.

The results show that MCS-PMFTSM has good fault tolerance under short-circuit fault.

4) MCS-PMFTSM CONCURRENT FAILURE OPERATION ANALYSIS

Concurrent faults mean that two or more different faults occur simultaneously within or between modules. The operation of the motor during the concurrent faults occurring within and between the modules are studied in this article.

a: CONCURRENT FAILURES WITHIN A MODULE

Two modules are operating normally. One has two-phase open circuits and one-phase short circuit, while the other has two-phase short circuits and one-phase open circuit. The phase current in the normal winding remains unchanged and the output torque of the motor is shown in Fig. 18.

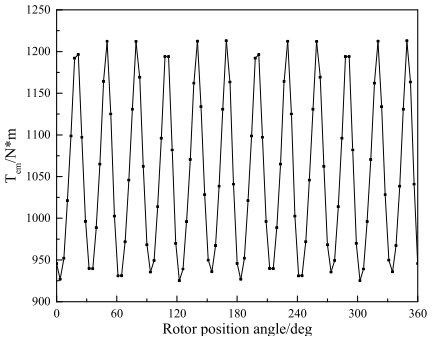

FIGURE 17. Rated torque output of the motor under three-phase short circuit.

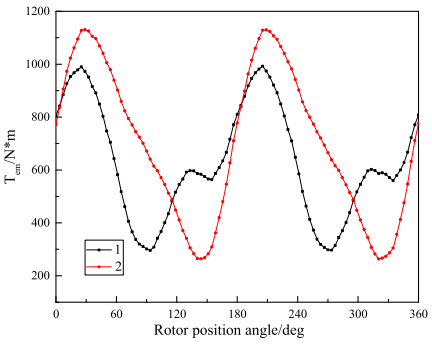

FIGURE 18. Output torque of the motor under one module concurrent failure(Phase current unchanged): 1-One phase-winding open circuit + two phase-winding short circuits Tavg = 629.1N*m; 2-Two phase-winding open circuits+ one phase-winding short circuit Tavg = 699.5N*m.

b: CONCURRENT FAULTS BETWEEN TWO MODULES

One module is operating normally. One module has an open circuit fault, whereas the other module has a one-phase short circuit, two-phase short circuits, and three-phase short circuits. The phase current in the healthy winding remains unchanged and the output torque of the motor is shown in Fig. 19.

As the number of short-circuit winding increases, the output torque decreases. This is because the number of short-circuit windings increases, while the braking torque has a greater impact. Additionally, the output torque of the motor decreases. Moreover, the output torque ripple of the three phase-winding short-circuits is less than one and two phase-winding short-circuits, which is consistent with the previous analysis results.

The worst concurrency fault is the condition that an open circuit of one module and the three-phase short-circuit of another module. At this time, the output torque of the motor is minimum. Considering the worst case, a genetic algorithm is used for optimization. The mathematical model of the optimization is given by Eq. (21).

$$\begin{cases} \max f(x) = T_{avg} \\ x = (I, \beta) \\ s.t. I \le 2.8I_N; 0° \le \beta \le 90° \end{cases} \tag{21}$$

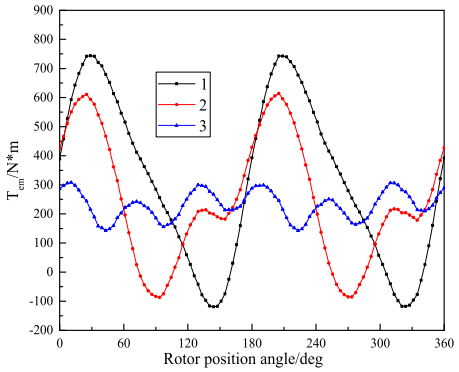

FIGURE 19. Output torque of the motor with concurrent faults between the two modules(Phase current unchanged): 1- One module open circuit+ one phase-winding short circuit Tavg = 313.9N*m; 2- One module open circuit + two phase-winding short circuits Tavg = 246.8N*m; 3- One module open circuit + three phase-winding short circuits Tavg = 230.5N*m.

Genetic algorithm is used to calculate the maximum torque output of the motor. The current amplitude is 2.8 times of the rated current. The phase current angle is 23.5°. The average value of the maximum torque is 793.5 N·m. The output torque of the motor is shown in Fig. 20.

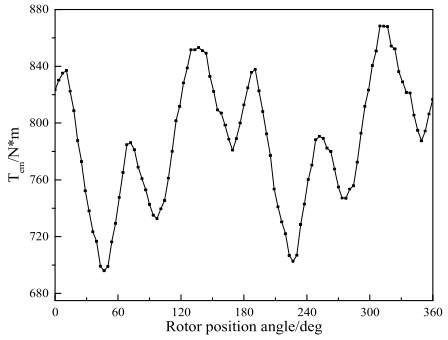

FIGURE 20. Output torque of the module under one module open circuit + one module three phase-winding short circuits (optimized).

In this condition, if the motor speed does not change, it cannot produce the rated torque due to the maximum operating temperature of the motor and the maximum current of the controller.

V. PROTOTYPE AND EXPERIMENT

The MCS-PMFTSM is manufactured. Some parameters of the prototype are given in Table 1. The structure of the MCS-PMFTSM is shown in Fig. 21 and and the experimental platform is shown in Fig. 22.

A. MEASUREMENT OF INDUCTANCE PARAMETERS

The measurements of the inductances of different types of motors are uniform. In this article, the three-phase inductance of the motor is measured according to the inductance measurement method given in a previous work [29]. The measured results of the MCS-PMFTSM self-inductance and mutual inductance are shown in Fig. 23.

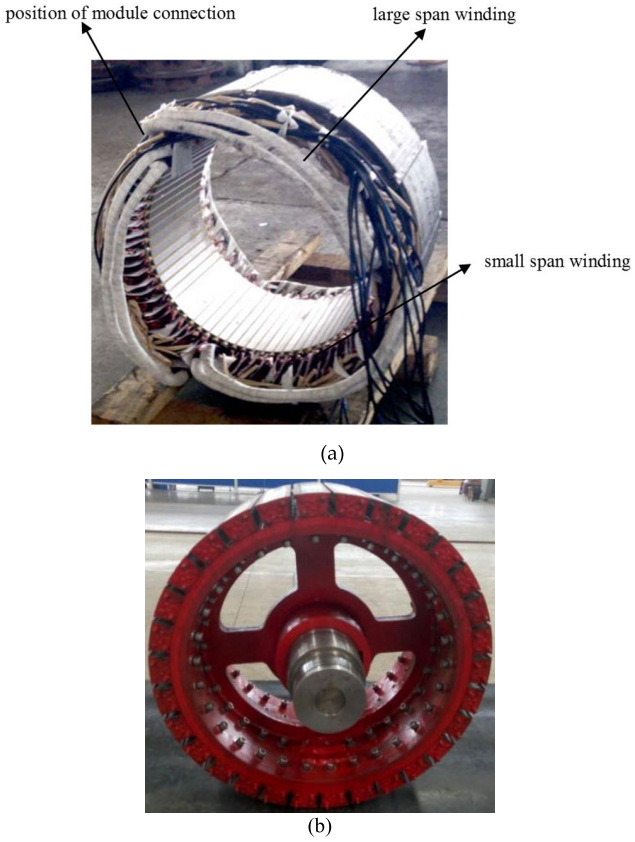

FIGURE 21. Prototype: (a) Stator (b) Rotor.

FIGURE 22. Experimental platform.

According to the inductance experiment results, the average value of the self-inductance of Phases A and C windings is 37.13 mH. The average value of the self-inductance of Phase B windings is 31.5 mH. The average value of the mutual inductance of the A and C windings is 10.28 mH. The average mutual inductance of Phases A and B is basically the same as that of Phases C and B. and has the value of 6.25 mH. The value of self-inductance and mutual inductance of phase windings with large-span is higher than that without the large-span coil phase windings, which is consistent with the previous analysis. The measurement results are similar to

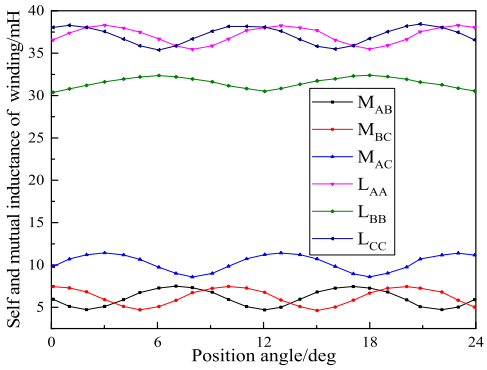

FIGURE 23. Inductance test data of the prototype.

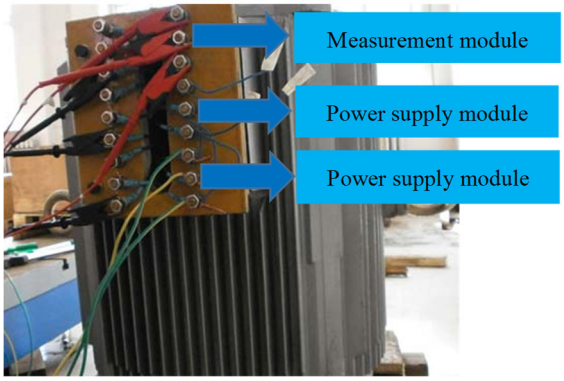

FIGURE 24. Prototype back EMF measurement.

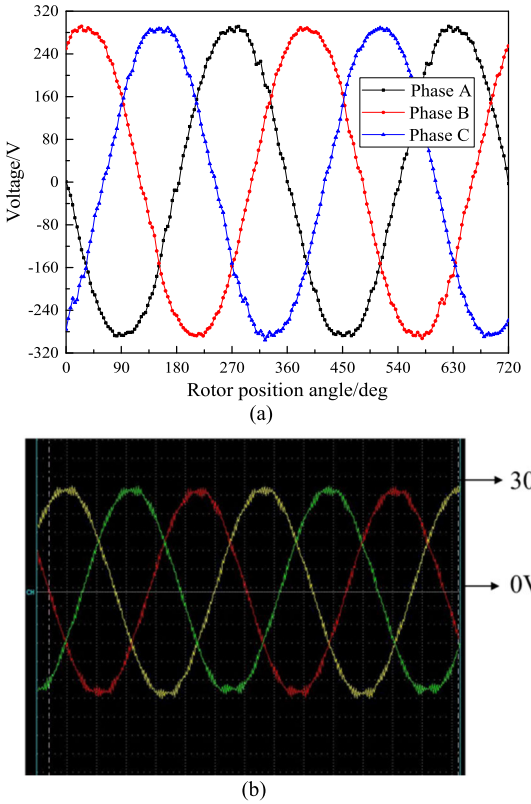

FIGURE 25. MCS-PMFTSM no-load back EMF waveform: (a) FEM calculation; (b) Measured.

the previous analysis results and prove the correctness of the previous analysis.

B. TEST OF NO-LOAD BACK EMF

In view of the particularity of the motor structure in this article, when measuring the back EMF of the motor, two module terminals are powered by the inverter, and one module terminal is connected to an oscilloscope for measurement. As shown in Fig. 24.

The measurement results and finite element method calculation results are shown in Figure 25. The finite element method calculation result of the no-load back EMF of the prototype is 210.2V, the measured value is 213.3V, and the error is only 1.4%. The measured no-load back-EMF waveform of the prototype is consistent with the FEM calculation results. This also indirectly proves that each module can be considered as a three-phase motor and the electromagnetic decoupling is realized between the modules.

C. HEALTHY OPERATION TEST

After removing the series inductance of Phase B, the phase of load current and load current of the MCS-PMFTSM are measured under rated working conditions, as shown in Fig. 26. Due to the limitation of experimental conditions, the total three-phase current of the motor system was measured. According to the MCS-PMFTSM structure, the current of each module should be 1/3 of the total current of the motor system. After conversion, the test result of the load current is close to that of the simulation. Because the parameters of the three-phase windings in the module are not equal, the two-phase currents of B and C have a phase offset angle of about 2° relative to the A-phase.

Due to machining accuracy, there is a certain difference between the two-phase currents of A and C, and the three-phase current is slightly larger than the value calculated by the FEM.

D. OPEN CIRCUIT FAULT OPERATION TEST

The inductances were connected to the B-phase winding of each module to balance the three phases. The open-circuit fault of the motor system is simulated by controlling the number of module motors in the operation. The phase current angle is certain and a different number of module motor operation is placed. The variation of the output torque of the motor system with the current is shown in Fig. 27.

When the motor is in one module and two faults, the output torque of the motor is close to the result of FEM analysis.

The motor system efficiency and the power factor were tested under rated speed, different load rates and a different number of running modules. The result are shown in Fig. 28.

It can be seen from the test curve results that the motor has high efficiency and high power factor at a load rate of more than 20% during normal operation. When the motor load

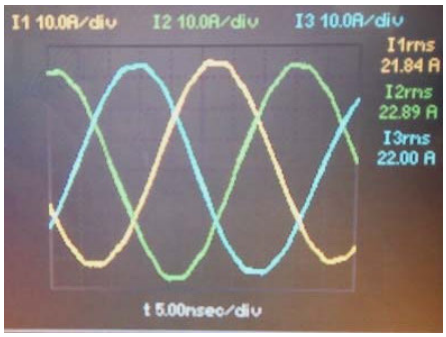

(a)

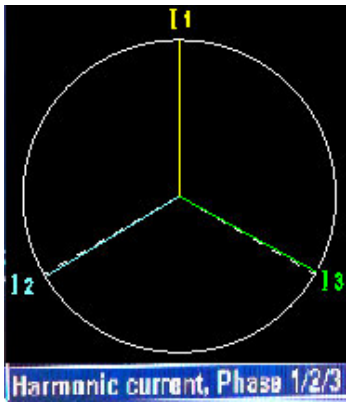

(b)

FIGURE 26. Rated current of prototype without series inductance: (a) Rated current RMS; (b) Rated load current phase.

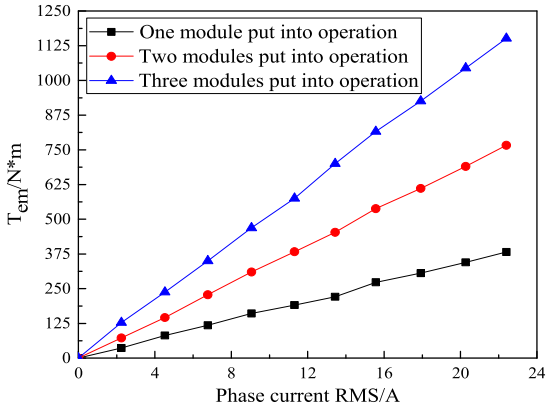

FIGURE 27. Torque output of the motor under different number of module motors operation.

rates and speed are constant, the motor operating efficiency decreases as the number of input modules decreases. The input electromagnetic power of the whole motor system is reduced with the reduction of the number of input modules, while the efficiency of the MCS-PMSM is reduced due to the increase of copper loss brought by the increase of input current. It can be seen from the above analysis that MCS-PMFTSM can still operate with strong fault tolerance after removing some modules.

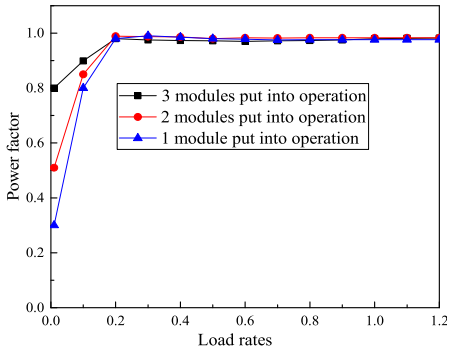

(a)

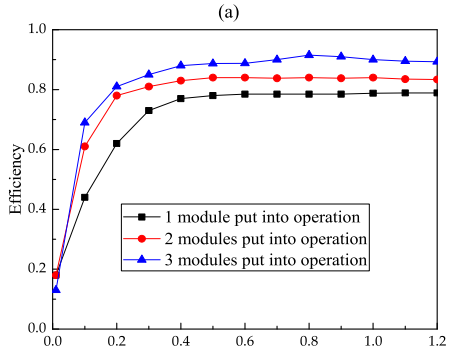

(b)

FIGURE 28. Efficiency and power factor of the prototype with different numbers of modules running at rated speed: (a) Power factor; (b) Efficiency.

VI. CONCLUSION

Since the span of the double-layer winding of the conventional modular fault-tolerant motor can only be 1, which limits the application of modular fault-tolerant motors. However the unequal span winding can solve this problem. The MCS-PMFTSM can realize the electrical decoupling and mechanical decoupling between the modules. The modules are controlled by independent inverters, whereas each module is a three-phase motor run unit. The unequal span winding structure and fault tolerance principle of MCS-PMFTSM are introduced in the work.Because there are two types of span coils in each module motor, the parameters of unequal span coils are calculated to provide a basis for analyzing the normal operation and fault-tolerant operation of MCS-PMFTSM. The performance of the motor under normal operation and various failure conditions are analyzed using finite element method. The results show that the motor has an excellent performance during normal operation. Under three kinds of fault conditions, the current control strategy is optimized by genetic algorithm. Therefore, the motor exhibits good performance during fault-tolerant operation. Finally, the rationality of the motor and the correctness of the analysis method are verified using experiments.

REFERENCES

[1] K.-H. Shin, J.-Y. Choi, and H.-W. Cho, "Characteristic analysis of interior permanent-magnet synchronous machine with fractional-slot concentrated winding considering nonlinear magnetic saturation," *IEEE Trans. Appl. Supercond.*, vol. 26, no. 4, pp. 1–4, Jun. 2016.

[2] B. Peng, W. Zhao, and X. Wang, "The method for reducing intrinsic shaft voltage by suitable selection of pole-arc coefficient in fractional-slot permanent-magnet synchronous machines," *IEEE Trans. Magn.*, vol. 54, no. 11, pp. 1–5, Nov. 2018.
[3] M. Abdelrahem, C. M. Hackl, and R. Kennel, "Finite position set-phase locked loop for sensorless control of direct-driven permanent-magnet synchronous generators," *IEEE Trans. Power Electron.*, vol. 33, no. 4, pp. 3097–3105, Apr. 2018.
[4] X. Zhu, X. Wang, C. Zhang, L. Wang, and W. Wu, "Design and analysis of a spoke-type hybrid permanent magnet motor for electric vehicles," *IEEE Trans. Magn.*, vol. 53, no. 11, pp. 1–4, Nov. 2017.
[5] G. Patterson, T. Koseki, Y. Aoyama, and K. Sako, "Simple modeling and prototype experiments for a new high-thrust low-speed permanent-magnet disk motor," *IEEE Trans. Ind. Appl.*, vol. 47, no. 1, pp. 65–71, Jan. 2011.
[6] Y. Gao, R. Qu, D. Li, and F. Chen, "Force ripple minimization of a linear Vernier permanent magnet machine for direct-drive servo applications," *IEEE Trans. Magn.*, vol. 53, no. 6, pp. 1–5, Jun. 2017.
[7] H. Zhou, G. Liu, W. Zhao, X. Yu, and M. Gao, "Dynamic performance improvement of five-phase permanent-magnet motor with short-circuit fault," *IEEE Trans. Ind. Electron.*, vol. 65, no. 1, pp. 145–155, Jan. 2018.
[8] L. Zhang, Y. Fan, R. Cui, R. D. Lorenz, and M. Cheng, "Fault-tolerant direct torque control of five-phase FTFSCW-IPM motor based on analogous three-phase SVPWM for electric vehicle applications," *IEEE Trans. Veh. Technol.*, vol. 67, no. 2, pp. 910–919, Feb. 2018.
[9] L. Xu, G. Liu, W. Zhao, J. Ji, and X. Fan, "High-performance fault tolerant Halbach permanent magnet Vernier machines for safety-critical applications," *IEEE Trans. Magn.*, vol. 52, no. 7, pp. 1–4, Jul. 2016.
[10] W. Zhao, T. A. Lipo, and B.-I. Kwon, "A novel dual-rotor, axial field, fault-tolerant flux-switching permanent magnet machine with high-torque performance," *IEEE Trans. Magn.*, vol. 51, no. 11, pp. 1–4, Nov. 2015.
[11] Y. Demir and M. Aydin, "A novel dual three-phase permanent magnet synchronous motor with asymmetric stator winding," *IEEE Trans. Magn.*, vol. 52, no. 7, pp. 1–5, Jul. 2016.
[12] X. Jiang, W. Huang, R. Cao, Z. Hao, J. Li, and W. Jiang, "Analysis of a dual-winding fault-tolerant permanent magnet machine drive for aerospace applications," *IEEE Trans. Magn.*, vol. 51, no. 11, pp. 1–4, Nov. 2015.
[13] X. Jiang, D. Xu, L. Gu, Q. Li, B. Xu, and Y. Li, "Short-circuit fault-tolerant operation of dual-winding permanent-magnet motor under the four-quadrant condition," *IEEE Trans. Ind. Electron.*, vol. 66, no. 9, pp. 6789–6798, Sep. 2019.
[14] G. Liu, M. Chen, W. Zhao, Q. Chen, and W. Zhao, "Design and analysis of five-phase fault-tolerant interior permanent-magnet Vernier machine," *IEEE Trans. Appl. Supercond.*, vol. 26, no. 4, pp. 1–5, Jun. 2016.
[15] L. Zhang, Y. Fan, C. Li, and C. Liu, "Design and analysis of a new six-phase fault-tolerant hybrid-excitation motor for electric vehicles," *IEEE Trans. Magn.*, vol. 51, no. 11, pp. 1–4, Nov. 2015.
[16] F. Li, W. Hua, M. Cheng, and G. Zhang, "Analysis of fault tolerant control for a nine-phase flux-switching permanent magnet machine," *IEEE Trans. Magn.*, vol. 50, no. 11, pp. 1–4, Nov. 2014.
[17] B. Tian, Q.-T. An, J.-D. Duan, D.-Y. Sun, L. Sun, and D. Semenov, "Decoupled modeling and nonlinear speed control for five-phase PM motor under single-phase open fault," *IEEE Trans. Power Electron.*, vol. 32, no. 7, pp. 5473–5486, Jul. 2017.
[18] Z. Song, Y. Yu, F. Chai, and Y. Tang, "Radial force and vibration calculation for modular permanent magnet synchronous machine with symmetrical and asymmetrical open-circuit faults," *IEEE Trans. Magn.*, vol. 54, no. 11, pp. 1–5, Nov. 2018.
[19] C. Tong, F. Wu, P. Zheng, B. Yu, Y. Sui, and L. Cheng, "Investigation of magnetically isolated multiphase modular permanent-magnet synchronous machinery series for wheel-driving electric vehicles," *IEEE Trans. Magn.*, vol. 50, no. 11, pp. 1–4, Nov. 2014.
[20] B. Wang, J. Wang, B. Sen, A. Griffo, Z. Sun, and E. Chong, "A fault-tolerant machine drive based on permanent magnet-assisted synchronous reluctance machine," *IEEE Trans. Ind. Appl.*, vol. 54, no. 2, pp. 1349–1359, Mar. 2018.
[21] P. Zheng, Y. Sui, J. Zhao, C. Tong, T. A. Lipo, and A. Wang, "Investigation of a novel five-phase modular permanent-magnet in-wheel motor," *IEEE Trans. Magn.*, vol. 47, no. 10, pp. 4084–4087, Oct. 2011.
[22] H. Lin, F. Zhao, and B. Kwon, "Analysis and control of the permanent magnet synchronous motor with auxiliary modular design," *IEEE Trans. Magn.*, vol. 54, no. 11, pp. 1–6, Nov. 2018.
[23] K. Atallah, J. Wang, and D. Howe, "Torque-ripple minimization in modular permanent-magnet brushless machines," *IEEE Trans. Ind. Appl.*, vol. 39, no. 6, pp. 1689–1695, Nov./Dec. 2003.
[24] K. Nounou, J. F. Charpentier, K. Marouani, M. Benbouzid, and A. Kheloui, "Emulation of an electric naval propulsion system based on a multiphase machine under healthy and faulty operating conditions," *IEEE Trans. Veh. Technol.*, vol. 67, no. 8, pp. 6895–6905, Aug. 2018.
[25] B. Zhang, B. Gan, and Q. Li, "Analysis of a fault-tolerant module-combined stator permanent magnet synchronous machine," *IEEE Access*, vol. 8, pp. 70438–70452, 2020.
[26] B. Dong, K. Wang, B. Han, and S. Zheng, "Thermal analysis and experimental validation of a 30 kW 60000 r/min high-speed permanent magnet motor with magnetic bearings," *IEEE Access*, vol. 7, pp. 92184–92192, 2019.
[27] J. F. Gieras, *Permanent Magnet Motor Technology: Design and Applications*. New York, NY, USA: CRC Press, 2010.
[28] C. Xia, S. Wang, X. Gu, Y. Yan, and T. Shi, "Direct torque control for VSI-PMSM using vector evaluation factor table," *IEEE Trans. Ind. Electron.*, vol. 63, no. 7, pp. 4571–4583, Jul. 2016.
[29] S. Yu, F. Zhang, and H. Wang, "Parameter calculation and analysis of a novel wind power generator," *IEEE Trans. Magn.*, vol. 53, no. 11, pp. 1–7, Nov. 2017.

BAOPING GAN received the B.S. degree in electrical engineering and automation from the Shenyang University of Technology, Shenyang, China, in 2016, where he is currently pursuing the Ph.D. degree in electrical engineering. His research interest includes design and control of permanent magnet motor.

BINGYI ZHANG received the B.S., M.S., and Ph.D. degrees in electrical engineering from the Shenyang University of Technology, Shenyang, China, in 1982, 1987, and 2007, respectively. He is currently a Professor with the Shenyang University of Technology. His research interests include design and optimization of electrical machines, low-speed high-torque drive systems, and power system automation.

QIAOSHAN LI received the B.S. degree in electrical engineering and automation from the Shenyang University of Technology, Shenyang, China, in 2015, where she is currently pursuing the Ph.D. degree in electrical engineering. Her research interest includes design and analysis of electrical machines.

FENG GUIHONG received the B.S. degree in electrical engineering from the Shenyang University of Technology, Shenyang, China, in 1985, and the M.S. degree in electric drive and automation from Northeastern University, Shenyang, in 1994. She is currently a Professor with the Shenyang University of Technology. Her research interests include design and optimization of electrical machines, low-speed high-torque drive systems, and power system automation.

GUANGKUO LI received the B.S. degree in electrical engineering and automation from the Shenyang University of Technology, Shenyang, China, in 2019, where he is currently pursuing the M.S. degree in electrical engineering. His research interest includes permanent magnet motor operation analysis.